SSC24-WVI-05

Horizontal Link Demonstration over 143 km with CubeISL: the World's Smallest Commercial Optical Communication Payload for Inter-Satellite Links

Jorge Rosano Nonay, René Rüddenklau, Benjamin Rödiger, Christopher Schmidt
Institute of Communications and Navigation (IKN), German Aerospace Center (DLR)
Münchener Straße 20, Weßling, 82234, Germany; +498153282411
jorge.rosanononay@dlr.de

Andreas Sinn, Georg Schitter
Automation and Control Institute (ACIN), TU Wien
Gusshausstrasse 27-29, Vienna, 1040, Austria

ABSTRACT

New developments in the field of free-space optical (FSO) communications are enabling a breakthrough in satellite miniaturization and data rates. The CubeISL laser communication terminal (LCT), developed by the German Aerospace Center (DLR), shall demonstrate in-orbit inter-satellite links (ISLs) at 100 Mbps and downlinks at 1 Gbps. When it launches in 2025, it aims to become the state-of-the-art technology for efficient CubeSat communications at high data rates and the world's smallest optical inter-satellite link terminal.

The performance of the CubeISL terminal was tested in a 143 km horizontal link between the islands of La Palma and Tenerife. In this setup, the transmitter from the LCT was used to characterize the atmospheric aberrations of the horizontal link using the ESA Optical Ground Station. Additionally, another LCT was used to demonstrate the tracking capabilities between two CubeISL terminals. This paper describes the current development status that allowed achieving an inter-island link. It analyzes the atmospheric aberrations encountered among the horizontal link and presents the results from the tracking performance between the two ISL terminals.

The focus of the paper lies specifically on the system's design which allows effortless transportation, swift assembly, and eye-safe operation. This design enables a pragmatic automatization of FSO links with CubeISL in flexible terminal–OGS configurations and campaign sites.

INTRODUCTION

Optical communication systems are enabling an unprecedented breakthrough in high-bandwidth satellite communication. Rapidly increasing data volumes are making traditional radio frequency (RF) channels less effective. Free-space optical (FSO) links offer higher bandwidth capabilities with significantly fewer regulations—unlike RF communication, which faces limitations due to the low availability of frequency channels. For similar data rates, optical systems also meet lower size, weight, and power (SWaP) requirements than their RF counterparts, enabling data throughput of gigabits per second (Gbps) even on the tiniest satellites.

Although the idea of optical communications in space was devised in the sixties, a successful downlink could not be achieved until 1995. CRL demonstrated a data rate of 1 Mbps with the ETS-VI satellite in a geosynchronous equatorial orbit (GEO).[1] In 2001, ESA demonstrated the first unidirectional optical inter-satellite link (ISL) at 50 Mbps using the Artemis satellite in GEO and the SPOT-4 satellite in low Earth orbit (LEO).[2] Bidirectional optical ISLs were first achieved in 2006 between ESA's Artemis and JAXA's OICETS satellites.[2] Since then, most efforts in FSO laser communications have evolved toward high data rate systems for large satellites—an ISL at 5.6 Gbps took place in 2008 using two of Tesat's laser communication terminals (LCT).[3] The increasing number of companies and organizations building satellite mega-constellations for global telecommunications (e.g., Starlink) is further pushing the development of commercial LCTs for direct-to-Earth (DTE) and inter-satellite links.[4] Private companies like Tesat-Spacecom or Mynaric already offer compact satellite terminals for FSO applications.

However, in recent years, a growing demand for high-speed links on CubeSats has started to shift this tendency, triggering significant progress on miniaturized FSO terminals. NICT was the first in 2014 to incorporate an LCT in a microsatellite on the SOCRATES mission.

It transmitted 10 Mbps on a LEO-to-Ground link.[5] NASA's OCSD program developed two 1.5U CubeSats, AeroCube-7B and -7C, which achieved optical downlinks of 200 Mbps in 2018.[6] The vehicles did not require any uplink beacon as they could rely only on their star tracker and attitude control system for stable satellite pointing. In 2022, MIT Lincoln Laboratory (MIT LL) and NASA's TBIRD demonstrated 200 Gbps DTE links from a 6U CubeSat in LEO.[7] The system sent >1 TB of error-free data in a single pass. As to optical inter-satellite links (OISLs), Spire Global launched two 3U technology demonstrator CubeSats and successfully demonstrated the transmission and detection of optical signals between them. They were followed in 2023 by two 6U CubeSats that will aim to relay data over OISLs.[8] In 2024, the CLICK B/C missions will attempt to demonstrate full-duplex OISLs at 20 Mbps between two 3U small spacecraft, in LEO over several hundred kilometers.[9]

The German Aerospace Center's Institute of Communications and Navigation (DLR-KN) also has a rich history of designing laser communication terminals for small satellites in LEO.[10] As part of its Optical Space Infrared Downlink System (OSIRIS) program, it developed the OSIRIS4CubeSat (O4C) LCT with a downlink speed of up to 100 Mbps. In 2023, it successfully demonstrated an end-to-end transmission to an optical ground station (OGS). Leveraging modular technology from O4C, DLR-IKN is developing CubeISL—a laser communication payload for LEO capable of bidirectional DTE and inter-satellite links. CubeISL is designed to cater to the growing demand for bandwidth on small satellites in LEO. The improved LCT shall be capable of downlinks at 1 Gbps, uplinks over 10 Mbps, and 100 Mbps ISLs at distances of up to 1,500 km. In 2025, two 6U CubeSats equipped with an LCT will fly in a mission led by DLR's Responsive Space Cluster Competence Center (RSC³).

The performance of the CubeISL terminal was tested in a 143 km horizontal link between the islands of La Palma and Tenerife. In this setup, the transmitter from the LCT in La Palma was used to characterize the atmospheric aberrations of the horizontal link using the ESA OGS in Tenerife. Additionally, another LCT was placed in Tenerife to demonstrate the tracking capabilities between two CubeISL terminals. This paper describes the current development status of the LCT that enabled an inter-island link. It focuses on the utilized setup and the alignment steps between the LCTs or the OGS. It analyzes the atmospheric aberrations encountered among the horizontal link and presents the results from the tracking performance between the two ISL terminals.

CUBEISL PAYLOAD

The CubeISL terminal is divided into three modules: the optical amplifier, the optical block, and the data and interface module. Its modular approach allows parallel development, testing, and integration of multiple subsystems. Each block occupies around one-third of a unit, as illustrated in Figure 1. The payload's volume of 1U thus complies with the CubeSat standard.

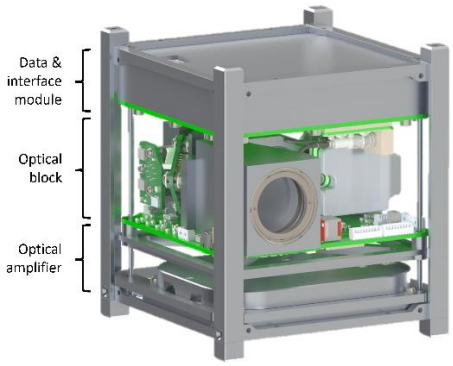

Figure 1: CAD Model of the CubeISL LCT.

The optical amplifier module consists of a commercial off-the-shelf (COTS) erbium-doped fiber amplifier (EDFA) with a maximum output of 1.3 W, although nominal operations shall be at 1.0 W. To evaluate its performance at the payload's end-of-life (EOL), the EDFA was irradiated with 23 krad(Si) total ionizing dose (TID) using a Gamma-ray source. Its electrical power consumption increased by 25%, corresponding to less than 15 W.[11]

The data and interface module encompasses the power distribution and control interface (PDCI) and a COTS data handling unit (DHU). The DHU gives the terminal almost absolute independence from the satellite and offers high flexibility for user-defined data processing, encoding, decoding, and storage. Fast-speed Ethernet and LVDS interfaces exchange data with the satellite's on-board computer (OBC) at 100 Mbps. It can store up to 2 Tbit of information and encode or decode the data with multiple forward error correction (FEC) codes (e.g., Reed-Solomon or LDPC).

The optical block, depicted in Figure 2, is the backbone of the CubeISL terminal. It uses the same optical path for the emitted (red) and the received (blue) beams. Light enters the system through a Keplerian beam expander with a 20 mm clear aperture (L_{TL1}) and a seven-fold magnification. After the expander, a micro-electro-mechanical system (MEMS) fast steering mirror (FSM) can displace the incoming beam by up to ±5 deg, which translates to a ±1 deg angular offset behind the aperture.

The light passes through the chromatic beamsplitter BS_1, which couples the emitter along the same optical path as the incoming beam. It is then focused, filtered, and split by a 30T/70R achromatic beamsplitter BS_2. The transmitted portion from BS_2 is used for the tracking loop, where a COTS 1 mm quadrant photodiode (QPD) and a microcontroller measure the beam's offset from the QPD's center and correct the alignment at a 200 Hz closed-loop bandwidth using the FSM. The long focal length gives the system a high resolution to compensate for minute offsets in the order of a few µrad. This feature—not mandatory during downlinks—is essential to minimize pointing losses in ISLs, especially if the terminals have small apertures. The reflected part of the beam at the BS_2 is focused again by a second focusing lens L_{FL2} that can be adjusted manually in three axes. This way, the spot can be simultaneously positioned at the center of the QPD and on the 200 µm avalanche photodiode (APD). The APD detector requires a sensitivity of ~1,000 photons per bit to read data at 100 Mbps.

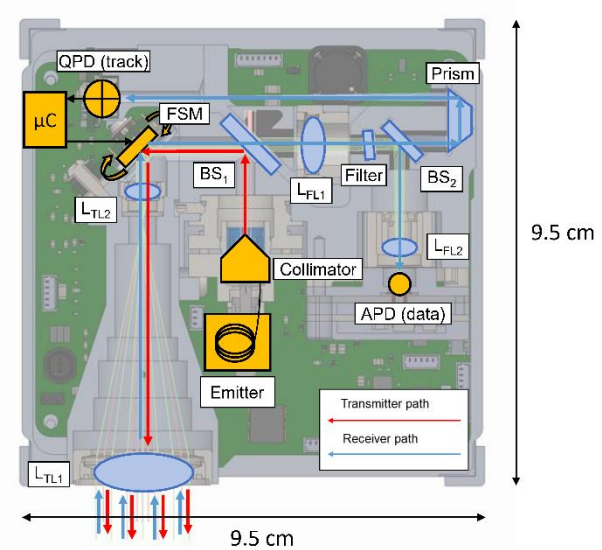

Figure 2: Schematics of the optical block. The red and blue paths depict the transmitted and received beam, respectively.

The optical system in Figure 2 is designed to spectrally isolate the received beam (Rx) of a few nanowatts from the up to 1.3 W emitted beam (Tx). Setting the emitted and received wavelengths 17 nm apart ensures that an Optical Density (OD) suppression of 9 of the emitter's wavelength is possible along the Rx path. However, spectral isolation requires two terminal configurations with opposing wavelengths: CubeISL(A) emits at 1537 nm and receives at 1553 nm, while CubeISL(B) emits at 1553 nm and receives at 1537 nm. Any terminal can only communicate with another terminal of the opposite type. The CubeISL in-orbit mission will thus consist of a payload of type A and one of type B to demonstrate an ISL. Both terminals have been designed to receive light at 1590 nm to remain compatible with the new Consultative Committee for Space Data Systems (CCSDS) O3K standard for optical systems.[12] Figure 2 shows a potential application for ISL and DTE links. It depicts a relay scenario where the two launched ISL terminals are used with two OGSs (demonstrating OGS interoperability). The scenario consists of an uplink via RF or in the future also optical, an optical ISL (OISL) between both terminals, and a downlink to a second OGS.

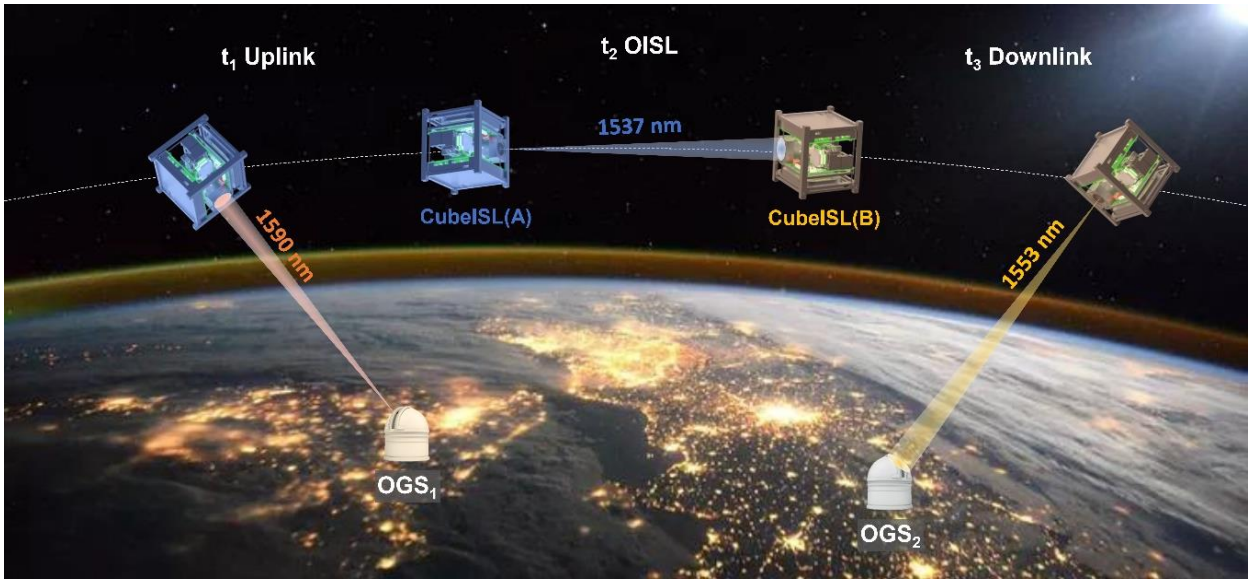

Figure 2: Possible in-orbit use case with two CubeISL terminals, where the terminals are used to relay data between two OGSs. It consists of an uplink, OISL, and downlink.

For CubeISL, an asymmetrical OISL acquisition scheme has been designed so that both terminals can start independently from each other without any need for synchronization. As shown in Figure 3, both terminals are initiated with their respective search patterns—which are precisely tailored to each other in terms of repetition period and appearance. While both patterns run continuously, the QPD detector is sampled at 1 kHz to identify any hit events from the opposing LCT. The terminals are differentiated in software as T-PAT (terminal for pointing, acquisition, and tracking) and T-DAT (terminal for detection, adjustment, and tracking). Once a hit occurs, each terminal determines the position error and adjusts its pointing. Now, the terminal T-PAT reduces the size of its search pattern while T-DAT falls into a holding position. With each new hit, the position is corrected by the measured position error in the subsequent holding phase. If T-DAT receives a constant signal that exceeds a specified dwell time, the system switches to closed-loop tracking mode. T-PAT directly switches to tracking mode when a signal is still present after the first hit. The holding phase can be exited after a defined waiting time, returning to the original search and breaking an impending infinite loop in the event of false positive hits. This acquisition design ensures that even in a constellation where satellites orbit in pairs of type A and B, the software only needs to know whether it should operate as CubeISL(T-PAT) or (T-DAT). This design makes both terminals—and schemes—interchangeable via software.

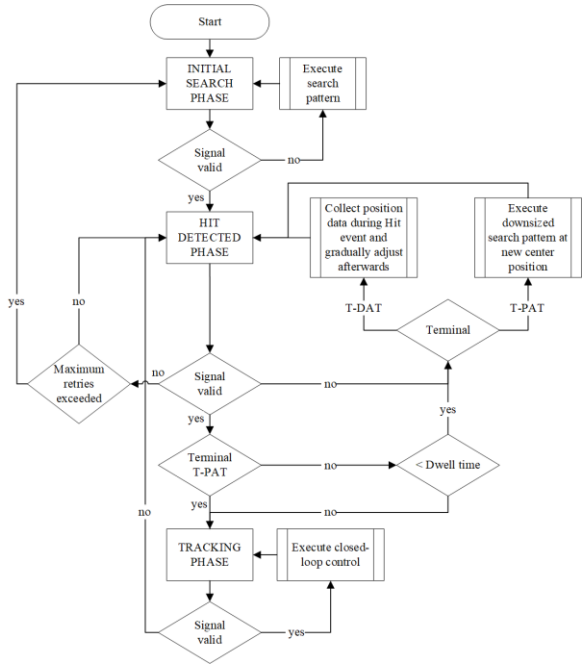

Figure 3: Flow chart describing the ISL acquisition scheme between the CubeISL(T-PAT) and (T-DAT) configurations.

HORIZONTAL LINK DESIGN

The 143 km horizontal FSO link was established between the observatories of La Palma and Tenerife on the Canary Islands. One CubeISL LCT was placed at the Jacobus Kapteyn telescope (JKT) in La Palma, and the second LCT was located at the ESA OGS in Tenerife, as seen in Figure 4. This link architecture has been previously used in multiple experiments, such as the record-breaking long-distance quantum entanglement.[13] Three experiments were successfully conducted during the CubeISL campaign: tracking with the LCT on the ESA OGS beacon simulating an uplink, an analysis of atmospheric aberrations along the horizontal link imitating a downlink, and the first successful tracking with the CubeISL LCT in an ISL configuration.

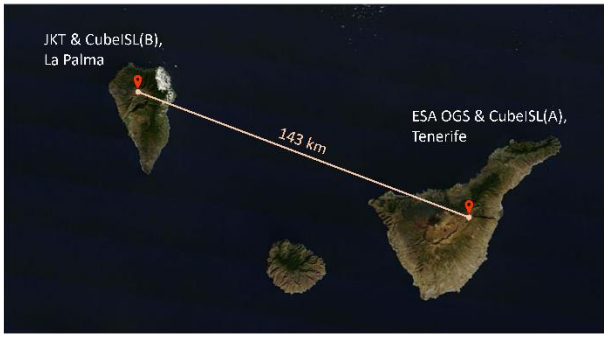

Figure 4: Architecture of the FSO link between the islands of La Palma and Tenerife.

Before the campaign, link budgets helped to verify the feasibility of each link. Table 1 shows the link budget for all three tests and consists of four sections: transmitter (Tx), channel (Ch), receiver (Rx), and budget (Bg). The emitter section lists the laser's output power, telescope gain (assuming a truncated, unobscured, and perfectly collimated telescope), losses from components, and a pointing penalty. At the channel, it accounts for the quadratic space loss and attenuation and scintillation losses from the atmosphere.[14-18] On the receiver section, the telescope gain is determined for either an unobscured LCT or the obscured OGS, with the optical loss and splitting loss accounting for its components and beamsplitters. The result is the available power at the detector surface. Lastly, the link margin assesses the difference between the power at the detector and the required power—during tracking, the LCT requires at least 250 pW (-66.0 dBm) of power. Both tracking experiments—i.e., uplink and ISL—show a large link margin of 30.7 and 7.5 dB, respectively, proving that the links are feasible with a significant buffer.[19]

Table 1: Horizontal link budget (values in dB).

Configuration:		LCT - OGS		LCT - LCT
Experiment:		Uplink Tracking	Downlink	ISL Tracking
Tx	Mean power	7.0	0.0	0.0
	Antenna gain	101.8	88.2	88.2
	Optical loss	-0.5	-0.3	-0.3
	Pointing loss	-1.0	-2.0	-2.0
Ch	Range loss	-241.1	-241.3	-241.4
	Atm. attenuation	-6.7	-7.1	-8.2
	Scintillation loss	-10.2	-2.6	-10.3
Rx	Antenna gain	92.1	125.6	92.2
	Optical loss	-1.5	-2.0	-1.5
	Splitting loss	-5.2	0.0	-5.2
Bg	Power at detector	-65.3	-41.5	-88.5
	Required power	-96.0	—	-96.0
	Link margin	30.7	—	7.5

In preparation for the campaign, a hermetic box was also designed that allows easy transportation, fast assembly, and, if required, eye-safe operations of the LCTs (see Figure 6). The box encompasses the LCT and its emitter—seed laser and EDFA. The emitter is attached to the top of the box and includes an Aluminum base plate to dissipate heat, evaluation hardware, and all necessary optical or electrical interfaces (the accessibility to the optical interfaces permits the easy attachment of optical attenuation components if required). A single opening for the laser beam is available in front of the LCT aperture. A removable OD2 absorption filter can be placed on the opening to comply with laser safety standards if required. A 3D-printed interface plate at the back of the boxes has feedthrough channels to provide power and exchange telemetry and telecommand (TM/TC) with all the systems inside the box. The interface plate also allocates an optical feedthrough interface to operate the LCT with other emitter subsystems. The practical box design allowed assembling and calibrating the LCTs in a controlled environment at Oberpfaffenhofen, safe transportation of all its sensitive components, and starting operations with the LCT at the campaign sites in a matter of hours by simply plugging in the necessary interfaces on the box.

During the campaign, the first experiment aimed to demonstrate the tracking capabilities of the CubeISL terminal simulating an uplink with the OGS. For this purpose, a 5W fiber laser module generates the beacon signal at 1590 nm. All beacon laser components are mounted directly to the telescope tube of the OGS (see Figure 5). Its output is modulated by a 10 kHz square

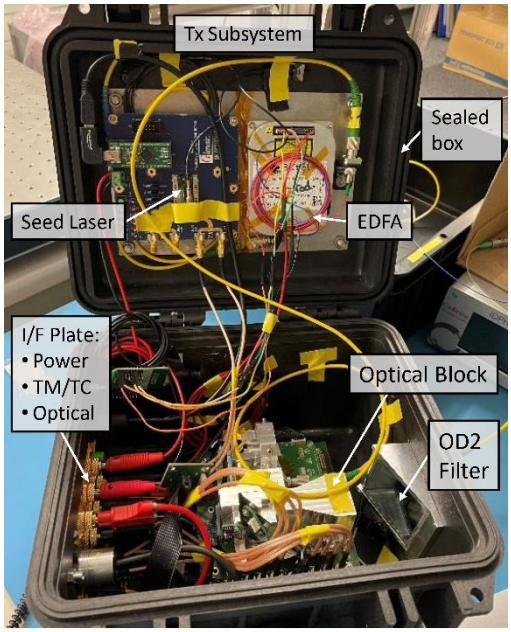

Figure 6: Hermetic box with the CubeISL terminal.

wave signal with a 50% duty cycle, and the beam is collimated with a 7 cm aperture collimator, resulting in a divergence angle of 560 µrad. Two motorized kinematic mirrors enable the co-alignment of the laser beacon to the OGS telescope. Characteristic landmarks served to support the multi-step alignment process at various distances. The individual landmarks are centered with the OGS using an InGaAs camera (C-RED 3, First Light Imaging, France). Then, the kinematic mirrors are moved systematically to align the spot of the laser beam to the center of the OGS.

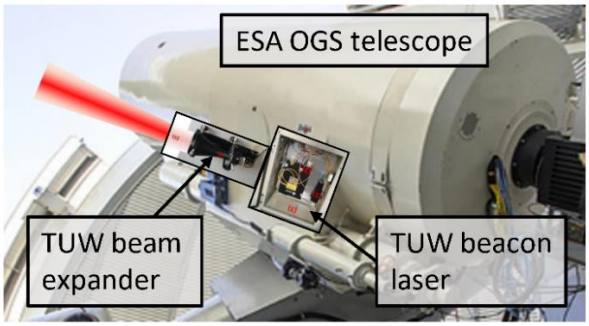

Figure 5: OGS Beacon and ESA OGS telescope.

The LCT in La Palma, shown in Figure 6, was mounted on a computerized telescope (10" f/10 LX200 ACF, Meade, USA) outside of the JKT telescope due to a lack of windows with direct line of sight to Tenerife. The setup with the motorized telescope allowed rotating the LCT in azimuth and elevation. The telescope's guide scope was used as visual feedback to establish an alignment between the emitter and the receiver on the neighboring island.

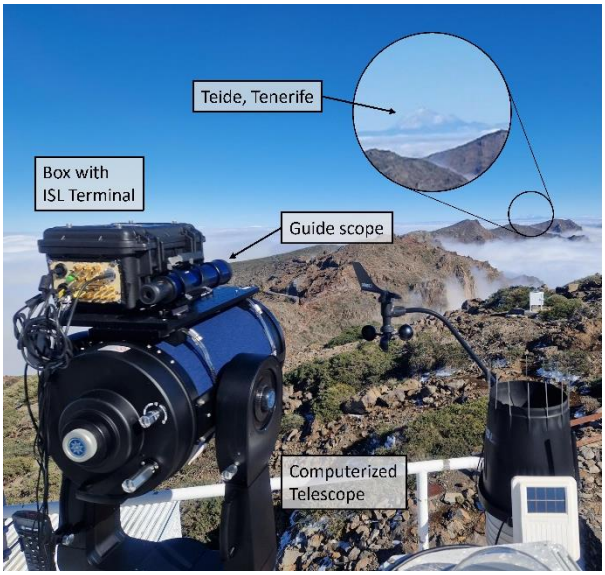

Figure 6: LCT located in La Palma, showing a close-up of Teide in Tenerife.

In Tenerife, the LCT was placed on top of a motorized goniometric elevation stage (LSDJ-15HW-02), a rotatory azimuthal stage (LSDH-200WS), and a manual adjustable height stage (L490/M, Thorlabs, USA) (see Figure 9). On top of them rested the LCT and guide scope (RS 4x32, Umarex, Germany). The LCT was placed in front of a window of the ESA OGS with direct visibility to the island of La Palma. A tripod was used to stabilize the whole setup. This configuration proved to be more efficient than the one in La Palma because it was sheltered inside and protected against wind gusts, which disturbed the pointing.

Once the terminals were set up on each island each LCT was aligned to its own guide scope. This process consisted of two steps: a coarse and a fine adjustment. The coarse alignment was made before the inter-island links were established to aid in finding the first light. For this step, the beam from the LCT was pointed toward a landmark 50 m away from the telescope. The process was verified with a short-wave infrared (SWIR) camera (XS-1.7-320, Xenics, Belgium). Then, the finderscope was aligned manually with the same landmark and tilted to compensate for the effect of parallax (at 50 m it accounts for ~0.3 deg). The terminal could then be aligned during the daytime with the neighboring island as shown in Figure 7 using the guide scope. The island's landmark was compared with a panorama constructed with an online tool that allows generating a panoramic view from any geographical point.[20] Upon coarse LCT pointing and alignment between the beacon on the OGS and the OGS telescope, the systems underwent the fine alignment procedure during the nighttime to point them to each other. First, the OGS and its beacon were pointed

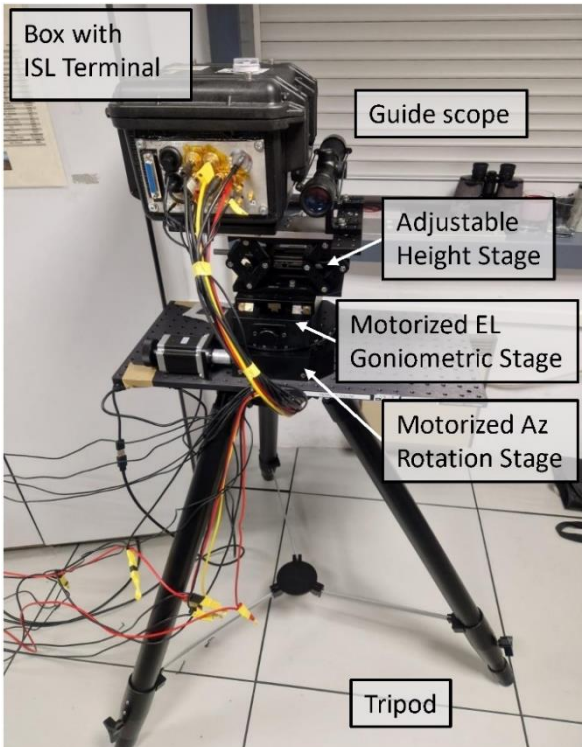

Figure 9: LCT located in Tenerife with two motorized Azimuth (Az) and Elevation (El) stages.

toward the neighbor island and its LCT. Their pointing was verified on La Palma with the SWIR camera. The LCT was first coarsely directed toward the OGS beacon using the motorized telescope until its alignment was within its field of regard (FOR) of ±1 deg. The LCT could then be aligned to the OGS using its closed-loop tracking scheme. This 143 km horizontal link at an altitude of 2.4 km represents a worst-case scenario for an uplink with the CubeISL terminal since the longer path along the atmosphere distorts the beam more than any expected uplink. It was verified using QCalc, a self-developed tool for computing link budgets.[21] Considering atmospheric-induced aberrations like scintillation and attenuation, a comparison between the horizontal and a DTE link at 5 deg elevation showed that the attenuation more than doubles. The higher scintillation index on the flat link also leads to a scintillation loss 2 dB higher than on the low elevation DTE link.

Upon reliable tracking between the LCT in La Palma and the OGS beacon, a quantization of the atmospheric aberrations along the horizontal link could be conducted at the OGS. Light at 1553 nm from the terminal's emitter was used at the Coudé optical bench of the ESA OGS to characterize the link's atmosphere and evaluate the performance of a tip-tilt compensation setup. Based on the link budget in Table 1, 71 µW (-41.5 dBW) of power

Figure 7: Alignment procedure of the LCT toward its target in La Palma. The first picture shows the finderscope. The second shows the view from the finderscope of the island of La Palma. The last picture superimposes a landmark panorama[20] over the island to show the exact position of JKT.

reached the optical bench at the OGS. For the entire duration of these measurements, stable tracking between LCT and OGS had to be maintained to reduce any errors induced by the emitter's pointing that could be confused with atmospheric aberrations. This horizontal experiment also represents a worst-case scenario compared to any downlink from orbit.

The last experiment succeeded in achieving the first tracking between two CubeISL terminals. In this setup, the LCT in Tenerife remained in a static position aligned toward the receiving LCT in La Palma. The LCT type A on Tenerife uses an emitter with 1.0 W at 1537 nm as a beacon. It stood on two elevation and goniometric stages held by a tripod to allow simple orientation in azimuth and elevation of the terminal. The breakdown of the link budget over the horizontal link can be seen in the right column of Table 1. A positive link margin verifies its feasibility. At the other end, the LCT type B in La Palma acquired the light from the emitter and reliably held the tracking. This experiment worked for initial pointing offsets of ±1 deg and during night and day thanks to the 10 kHz modulation of the emitter signal.

RESULTS

Several improvements to the terminal's design and performance were needed to perform an inter-island link. The optomechanical design was optimized regarding the quality of the spot at the QPD to achieve the best performance. The tracking performance was evaluated for different modulated signals. As shown in Table 1, the link margin for the ISL tracking scenario is greater than 3 dB.

After characterizing the mentioned LCT's main functionalities in a controlled environment in Oberpfaffenhofen, the systems were transported and prepared for the horizontal inter-island link test. Here, three different experiments were performed:

- Uplink tracking from the OGS beacon to the LCT.
- Downlink from the LCT to the OGS telescope.
- Unidirectional tracking in ISL configuration between two LCTs.

Tracking on ESA OGS – Uplink

With the initial conditions described in the Section *Horizontal Link Design*, it was possible to start the PAT procedure on the LCT. Links were performed and recorded from 04:09 am until the last link at 21:58. Table 2 shows the results for four OGS links during different background lighting conditions. All measurements operated in closed-loop tracking mode—where μ_{FSM} shows the normalized offset from a perfect alignment. The tracking error, σ_{error}, indicates the performance of the LCT. Values smaller than 20 µrad are considered optimal tracking performance, and below 40 µrad it is still acceptable for operation. Therefore, all links fulfill the requirements for data transmission. The last column indicates the effect of wind acting on the LCT measured by the on-board gyroscopes.

Table 2: LCT tracking performance on ESA OGS.

Scenario	μ_{FSM}, deg	σ_{error}, µrad	σ_{gyro}, µrad/s
OGS 04:09	0.123	3.38	2.09
OGS 17:00	0.123	18.21	15.36
OGS 18:44	0.165	36.40	62.83
OGS 21:58	0.159	12.71	52.36

Atmospheric Characterization – Downlink

This experiment evaluates the atmospheric turbulence affecting the horizontal link and the corresponding potential of tip-tilt compensation to counteract these disturbances. The tip-tilt compensation loop is formed by a QPD (InGaAs3000, OSI Optoelectronics, USA) and an FSM (FSM3000, Micro-Epsilon, Germany), enabling a closed-loop compensation bandwidth of up to 1 kHz with an FPGA-based real-time system. Additionally, a custom-assembled wavefront sensor (WFS) consisting of a fast NIR camera (C-RED 3) running at 600 frames per second and a lenslet array with 20x20 lenslets and 0.36 mm pitch is integrated to record the distribution of higher-order aberrations.

Using the beacon laser at the ESA OGS, an inter-island link is established with the CubeISL LCT at La Palma. The Tx laser beam from the LCT acts as a reference to conduct measurements using the QPD and the WFS. Figure 7 shows the spatial atmospheric statistics recorded over time using a modal representation captured at 4:57 am. During the first five seconds, no

compensation is active, and a clear dominance of low-order aberrations is visible. At second five, the compensation loop is closed, reducing the tip-tilt RMS errors by up to a factor of 10 to 0.61 µrad and 0.65 µrad, respectively. The total RMS wavefront error decreases by a factor of 1.8, which indicates a 44% contribution of tip and tilt aberrations to the wavefront error. Despite a receiving aperture of 1 m, the scintillation index reached the strong scintillation regime with values ranging up to 2.23.

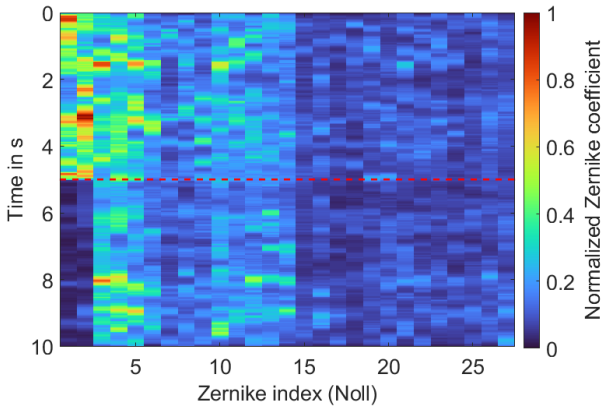

Figure 7: Measured Zernike distribution over time of the horizontal link. From 0 to 5 seconds, tip-tilt compensation is disabled. After 5 seconds, it is enabled (red dashed line) and the contribution of tip and tilt aberrations are reduced significantly.

Tracking on a CubeISL LCT – ISL

This experiment aimed to identify whether the residual error could be estimated using search patterns and—in case this is possible—how accurate the results are to the tracking reference. This approach is relevant because the developed ISL acquisition scheme (see Figure 3) relies on the assumption that the current alignment is corrected after at least one hit so that the two LCTs can converge gradually. However, the lack of an independent angle measurement sensor on its FSM introduces additional uncertainty to the search process. The results from the unidirectional inter-CubeISL link in Table 3 were used to verify this hypothesis. Due to the limited available link time—affected by thick clouds blocking the inter-island link view—only one reference measurement could be performed for each acquisition pattern (i.e., grid, spiral, rose, and Lissajous).

Table 3: Unidirectional tracking with two LCTs.

Scenario	μ_{FSM}, deg	σ_{error}, µrad	σ_{gyro}, µrad/s
ISL 18:17	0.121	29.17	38.40

A comparison of the attitude error estimation between the beacon of the OGS and the beacon of the CubeISL terminal can be seen in Figure 8. The best results in both cases were achieved with the grid pattern, probably because the system is in motion for all other acquisition patterns. The OGS acquisition run started at 16:34 and resulted in a measurement error of $1.056 \cdot 10^{-4}$ rad to the reference point. The ISL link was performed at 19:41 with a deviation of $6.104 \cdot 10^{-5}$ rad between tracking reference and attitude derived by the acquisition hits. Despite the atmospheric turbulence and attenuation between the two islands, the LCT proved that it could acquire, establish, and hold a link in all experiments with the ESA-OGS or another CubeISL terminal.

(a) CubeISL(A) with OGS beacon

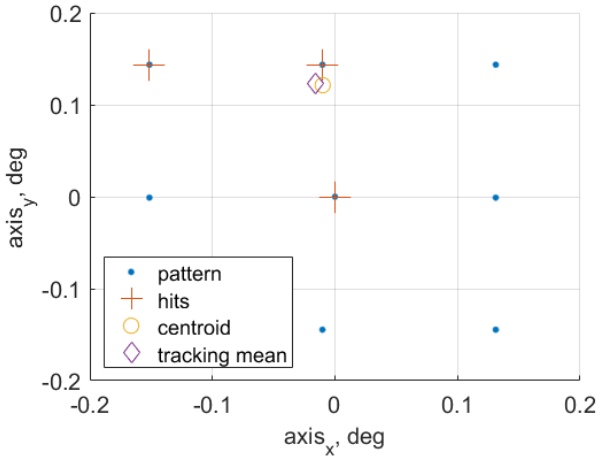

(b) CubeISL(A) with CubeISL(B) beacon.

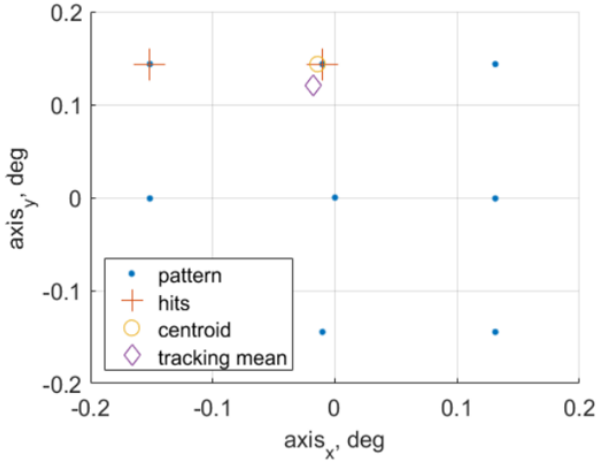

Figure 8: Comparison of the attitude error estimation during the acquisition phase between an LCT with the OGS and for an ISL. The blue dots represent the FSM positions of CubeISL(A) in a grid pattern, and those with a target hit are marked with a red cross. The derived centroid and the measured tracking-reference positions are shown as a yellow circle and a purple diamond, respectively.

CONCLUSIONS

In 2025, two CubeISL payloads shall demonstrate downlinks with an OGS at 1 Gbps, bidirectional ISLs over 1,500 km at 100 Mbps, and DTE interoperability with multiple OGSs. The first field campaign has verified the tracking performance of one LCT with an OGS and another LCT. The campaign took place in the Canary Islands between the observatories of Tenerife and La Palma. The 143 km horizontal inter-island link represents a worst-case scenario for the ISL and DTE links that the payloads will experience from orbit.

This paper dives deep into the payload design, tracking architecture of the CubeISL terminal, and setup used during the inter-island link campaign. The results from the campaign in all three experiments (i.e., tracking on an OGS, atmospheric characterization of the link, and tracking on an LCT) verify the high reliability and performance of the CubeISL payloads. All links established with the ESA OGS showed that the PAT procedure was within the tracking error range of optimal tracking (e.g., <20 µrad). With this setup, it was possible to use the Tx signal from the LCT in La Palma to characterize the atmospheric channel along the horizontal link between the islands. The tip-tilt compensation loop allows a reduction of 44% in the contribution of atmospheric aberrations to the signal's wavefront error. Finally, the unidirectional inter-CubeISL link successfully verified the assumptions the ISL acquisition scheme relies on. The accuracy of the attitude error estimation on ISL and DTE links proved that it could acquire, establish, and hold a link over 143 km despite any atmospheric aberrations.

The architecture used on the inter-island link allows for straightforward automatization of the whole link establishment procedure between two compatible systems (LCTs or OGSs). This is especially relevant for the CubeISL terminal where the ISL tracking scheme involves a complex alignment procedure and high test-repetition frequency to obtain relevant data for all the proposed tracking patterns (i.e., spiral, grid, rose, and Lissajous). The upcoming steps in the CubeISL development will focus on establishing a reliable bidirectional link between two LCTs—tracking actively on each other—in an end-to-end test of the ISL PAT scheme. For this test, an automatization procedure is already being implemented that will allow full autonomy to establish ISLs between the LCTs. Once the APD (i.e., data receiver) has been characterized and its focusing mechanism qualified for space applications, a campaign will validate data transmission at 100 Mbps in an ISL configuration. These tests will mark the final milestones in the development of CubeISL—the world's smallest commercial optical inter-satellite link terminal.

ACKNOWLEDGEMENTS

The authors would like to thank the Institute of Astrophysics of the Canary Islands (IAC) in La Laguna, Tenerife for granting access to their telescopes, and especially Jorge Socas, Juan Carlos Perez, and Luis Fernando Rodriguez for their support. The project CubeISL is supported by the German Federal Ministry of Defense through the technological research and development assignment Responsive Space Capabilities.

REFERENCES

1. K. Araki, Y. Arimoto, M. Shikatani, M. Toyoda, M. Toyoshima, T. Takahashi, S. Kanda, and K. Shiratama, “Performance evaluation of laser communication equipment onboard the ETS-VI satellite,” in Photonics West, (1996).
2. S. Kuzkov, Z. Sodnik, and V. Kuzkov, “Laser communication experiments with ARTEMIS satellite,” in Proceedings of the International Astronautical Congress, IAC, vol. 4 (2013).
3. B. Smutny, H. Kaempfner, G. Muehlnikel, U. Sterr, B. Wandernoth, F. Heine, U. Hildebrand, D. Dallmann, M. Reinhardt, A. Freier, R. Lange, K. Boehmer, T. Feldhaus, J. Mueller, A. Weichert, P. Greulich, S. Seel, R. Meyer, and R. Czichy, “5.6 Gbps optical intersatellite communication link,” in Free-Space Laser Communication Technologies XXI, vol. 7199 H. Hemmati, ed., International Society for Optics and Photonics (SPIE, 2009), p. 719906.
4. A. U. Chaudhry and H. Yanikomeroglu, “Laser intersatellite links in a Starlink constellation: A classification and analysis,” IEEE Veh. Technol. Mag. 16, 48–56 (2021).
5. A. Carrasco-Casado, H. Takenaka, D. Kolev, Y. Munemasa, H. Kunimori, K. Suzuki, T. Fuse, T. Kubo-Oka, M. Akioka, Y. Koyama, and M. Toyoshima, “LEO-to-ground optical communications using SOTA (Small Optical TrAnsponder) – payload verification results and experiments on space quantum communications,” Acta Astronaut. 139, 377–384 (2017).
6. T. S. Rose, D. W. Rowen, S. D. LaLumondiere, N. I. Werner, R. Linares, A. C. Faler, J. M. Wicker, C. M. Coffman, G. A. Maul, D. H. Chien, A. C. Utter, R. P. Welle, and S. W. Janson, “Optical communications downlink from a low-earth orbiting 1.5U CubeSat,” Opt. Express 27, 24382–24392 (2019).
7. C. M. Schieler, K. M. Riesing, B. C. Bilyeu, B. S. Robinson, J. P. Wang, W. T. Roberts, and S. Piazzolla, “TBIRD 200-Gbps CubeSat downlink: System architecture and mission plan,” in 2022

IEEE International Conference on Space Optical Systems and Applications (ICSOS), (2022), pp. 181–185.

8. Spire Global, "Spire launches industry-leading technology to enable optical inter-satellite links and significantly reduce data latency - spire: Global data and analytics," https://spire.com/press-release/spire-launches-industry-leading-technology-to-enable-optical-inter-satellite-links-and-significantly-reduce-data-latency/ (2023).
9. NASA, "Cubesat laser infrared crosslink," https://www.nasa.gov/smallspacecraft/what-is-click/ (2023).
10. C. Schmidt, B. Rödiger, J. R. Nonay, C. Papadopoulos, M.-T. Hahn, F. Moll, and C. Fuchs, "DLR's optical communication terminals for CubeSats," in 2022 IEEE International Conference on Space Optical Systems and Applications (ICSOS), (2022), pp. 175–180.
11. B. Rödiger, J. R. Nonay, C. Roubal, R. Rüddenklau, C. Schmidt, and J. P. Jakobs, "Qualification of inter-satellite link laser communication terminals on CubeSats - CubeISL," in Small Satellite Conference (SmallSat) 2023, (2023).
12. CCSDS 141.0-B-1, Optical Communications Physical Layer + Pink Sheets (2020).
13. T. Herbst, T. Scheidl, M. Fink, J. Handsteiner, B. Wittmann, R. Ursin, and A. Zeilinger, "Teleportation of entanglement over 143 km," Proc. Natl. Acad. Sci. 112, 14202–14205 (2015).
14. L. C. Andrews and R. L. Phillips, Laser Beam Propagation through Random Media, Second Edition (SPIE—The International Society for Optical Engineering, Bellingham, 2005).
15. N. Das, Optical Communications Systems (IntechOpen, Rijeka, 2012).
16. H. Hemmati, Near-Earth Laser Communications, Second Edition, Optical Science and Engineering (CRC Press, 2020).
17. J. R. Nonay, C. Fuchs, D. Orsucci, C. Schmidt, and D. Giggenbach, "Seleniris: a moon-earth optical communication terminal for CubeSats," in 2022 IEEE International Conference on Space Optical Systems and Applications (ICSOS), (2022), pp. 186–195.
18. D. Giggenbach and H. Henniger, "Fading-loss assessment in atmospheric free-space optical communication links with on-off keying," Opt. Eng. 47, 046001 (2008).
19. J. R. Nonay, R. Rüddenklau, A. Sinn, J. P. Jakobs, J. Berlitz, B. Rödiger, and G. Schitter, "Horizontal free-space optical link with CubeISL over 143 km," J. Opt. Commun. Netw. 16, 593-601 (2024).
20. U. Deuschle, "Generate a Panorama," https://www.udeuschle.de/panoramas/makepanoramas_en.htm (2023).
21. D. Orsucci, J. R. Nonay, A. Shrestha, and F. Moll, "QCalc: a tool to compute classical and quantum communication rates over free-space optical channels," in Emerging Imaging and Sensing Technologies for Security and Defence VI, vol. 11868 G. S. Buller, R. C. Hollins, R. A. Lamb, and M. Laurenzis, eds., International Society for Optics and Photonics (SPIE, 2021), p. 118680F.